Mobile polaron solutions and nonlinear electron transfer in helical protein models

Dirk Hennig
Freie Universität Berlin, Fachbereich Physik, Institut für Theoretische Physik, Arnimallee 14, 14195 Berlin, Germany
(Received 15 February 2001; revised manuscript received 6 June 2001; published 21 September 2001)

We consider the electron transfer along helical forms of proteins. The spatial structure of the protein helices is modeled by three-dimensional oscillator networks whose constituents represent peptide groups. Covalent and hydrogen bonds between the peptide units are modeled by point-point interaction potentials. The electronic degree of freedom is described by a tight-binding system including besides the nearest-neighbor exchange interactions between covalently connected units also third- or fourth-nearest neighbor interactions between hydrogen-bonded sites. In addition each peptide unit possesses an internal vibrational degree of freedom. The various dynamical degrees of freedom are coupled to each other making the exchange of electronic, intramolecular, and bond-vibrational energy possible. In the first part of the paper we investigate the static polaron formation resulting from strong interactions between the electron and the intramolecular vibrations. The 3-10 helix and the α helix are investigated. Polaron states are constructed analytically on the basis of a variational approach. Compared to the α helix the 3-10 helix supports stronger localized polarons. In the second part of the paper we take the coupling of the polaron with the vibrations of the three-dimensional protein matrix into account focusing interest on the bond-assisted initiation of polaron motion. In detail it is demonstrated that the interplay of the protein matrix and the polaron dynamics conspire to activate not only the polaron motion but also to maintain a long-lived coherently traveling localized pattern along the lattice of peptide units. Starting from a nonequilibrium state it is shown that coexisting electron and bond-vibration breathers assist the relaxation dynamics towards energy equilibration and the attainment of a stationary regime.

DOI: 10.1103/PhysRevE.64.041908 PACS number(s): 87.15.−v, 63.20.Ry, 63.20.Pw, 63.20.Kr

I. INTRODUCTION

Excitation energy transfer processes in biological systems are problems of long-standing interest [1–3], and especially the functional primary processes in photosynthetic reaction centers, drug metabolism, cell respiration, enzyme activities, and gene regulation have been studied intensively. In this context understanding the mechanism of electron transfer (ET) in proteins has attracted considerable attention during the last years [4,5]. The exploitation of the ET processes to construct technological devices has already been proposed [6,7] and for such an achievement a theoretical understanding of the transfer mechanism is needed.

Inspired by the success of protein modifications along with the determination of their three-dimensional structure microscopic theories for protein-energy-transfer reactions were developed. Data of high resolving x-ray analysis of proteins gave the essential details on an atomic scale needed as input quantities for microscopic theories of ET in proteins. This gave insight into the relation between the structure and function for the energy and particle transfer in proteins [8–10] and it was shown how the steric structure of proteins can affect the electron tunneling [11,12]. In particular, as verified by recent experiments [13], the H bridges involved in the protein secondary structure are vital for mediating ET in proteins. In fact under physiological conditions the ET may be activated by couplings to vibrational motion [6]. Furthermore, molecular dynamics simulations [14] have predicted that global protein motions are very important for biochemical reactions, for instance, in light-induced reactions of chromophores accompanied by nuclear motions and for the ET in pigment protein complexes. In reaction center proteins proceed the protein nuclear motions coherently along the reaction coordinate on the picoseconds time scale of ET as femtosecond spectroscopy revealed [15]. Thus the vibrational dynamics of proteins may serve as the driving force of ET in proteins. In the current work we investigate a nonlinear electron (actually polaron) transport mechanism relying on the mutual coupling between the electron amplitude and intramolecular respectively bond vibrations in proteins. Studies of energy storage and transport in biomacromolecules on the basis of self-trapped states have a long history beginning with the work of Landau [16] and Pekar [17]. They introduced the concept of a polaron, i.e., an electron accompanied by its own lattice distortion forming a localized quasiparticle compound. When the size of the polaron is large enough so that the continuum approximation can be applied to the underlying lattice system Davydov [18,19] and Davydov and Kislukha [18] has shown that a mobile self-trapped state can travel as a solitary wave along the molecular structure. Since the work of Davydov the relevance of solitons for the energy and particle transport in biomolecules has been recognized and has remained of great interest (see, e.g., [20–22]). Most of the studies of transport properties in biopolymers are based on one-dimensional nonlinear lattice models, and recent two- and three-dimensional extensions with respect to solitonic transport of vibrational energy can be found, e.g., in [23–25]. The theory of nonlinear ET mechanism in one-dimensional chain models of proteins is described in [19,22] and recent considerations demonstrate that supersonic acoustic solitons can capture and transfer self-trapping modes in anharmonic one-dimensional lattices [26]. Regarding the enforcing role played by soliton motion in the functional processes in biomolecules we note that in a recent work it has been proposed that the folding and conformation process of proteins may be mediated by solitons traveling along the

polypeptide chains while interacting with a field corresponding to the conformation angles of the protein [27]. Furthermore, in a nonlinear dynamics approach to DNA dynamics it has been suggested that solitons propagating along the DNA molecule may play an important role in the denaturation and transcription process [28–30].

For a theoretical understanding of protein ET mechanisms the corresponding models should not only incorporate the static aspect of the protein structure but also its dynamics (see [31] and references therein). In particular, it has been illustrated that the dynamical coupling of a moving electron to vibrational motions of the peptide matrix can lead to some biological reactions in an activationless fashion [32]. The following investigation is devoted to bond-mediated protein ET using the concept of breather solutions. We consider the transfer of an electron along folded polypeptide chains arranged in three-dimensional conformations constituting the secondary helix structure of the proteins. We investigate the transfer properties of two common types of helices, namely, the α and 3-10 helix, respectively. The secondary helix structure is modeled by a three-dimensional network the constituents of which are the peptide groups. The peptide units are connected via point-point pair-potentials modeling the covalent and hydrogen-bond interactions, respectively. The electronic system is described by a tight-binding lattice. It is assumed that each peptide unit possesses one internal (intramolecular) vibrational degree of freedom represented by the C═O stretching mode, that is, the amide-I vibrations. Strong couplings between the electron amplitude and intramolecular vibrations lead to polaron formation. Moreover, we demonstrate that the coupling between the polaron and the vibrations of the protein matrix can activate coherent polaron motion.

In the first part of the paper we study the polaron problem consisting of the electronic degree of freedom strongly coupled to intramolecular vibrations. We construct stationary polaron states in two different ways. First results regarding the extension, bistability, energetic content and pattern of polaron states are analytically gained from a variational approach. Subsequently we numerically derive the ''exact'' polaron states with the help of a corresponding map. In particular we explore the impact of the longer-range dispersion related to hydrogen-bonded units on the localization features. We perform a normal mode analysis for the polarons, classify their internal localized modes, and discuss modifications due to larger dispersive interaction radius. Finally we consider the possibility to initiate the mobility of a polaron by suitable excitation of a pinning mode.

The second part of the paper deals with the coupled problem for which the vibrations of the steric protein matrix are incorporated into the polaron dynamics. We are interested in the relaxation dynamics when the system starts in a nonequilibrium initial state. Such nonequilibrium states occur in the presence of a localized electron (exciton) produced spontaneously or experimentally through initial phototransfer excitation. Special attention is paid to a possible activation of polaron motion coupled to the vibrational dynamics of the peptide units in the three-dimensional secondary structure. We show that the formation of breatherlike bond vibrations coexisting with a moving electron breather play a crucial role for long-lived coherent ET. Finally, in Sec. V we give a summary of our results.

II. THE HELIX PROTEIN MODEL

We discuss the ET along two different types of helices of proteins. A helix is formed when the primary structure of the one-dimensional sequence of linearly linked amino acid residues is tightly curled about its longitudinal axis. The resulting secondary structure is stabilized by hydrogen bonds formed between the carbonyl oxygen of residue n and the amide hydrogen of residue $n+m$ resulting in m spines of H-bonded residues that span the length of the helix. We consider the 3-10 helix arising when a residue forms a hydrogen bond with a residue that is three residues away and the α helix for which residues being four sites apart from each other are linked through a hydrogen bond.

Concerning ET the electronic part of the Hamiltonian is given by

$$H_e=\sum_n \sum_\mu \epsilon_{n\mu}|c_{n\mu}|^2-\sum_n \sum_\mu V_{\mu+1\mu}[c^*_{n\mu+1}c_{n\mu} + c_{n\mu+1}c^*_{n\mu}]-\sum_n \sum_\mu W_{n+1n}[c^*_{n+1\mu}c_{n\mu}+c_{n+1\mu}c^*_{n\mu}], \tag{1}$$

where $c_{n\mu}$ is the probability to find the electron at the site (peptide unit) $(n\mu)$. $V_{\mu+1\,\mu}$ designates the interchain transfer matrix element responsible for the ET between covalent-bonded peptide units with the periodicity condition $c_{n,\mu=3}=c_{n+1,\mu=1}$ for the 3-10 helix and $c_{n,\mu=4}=c_{n+1,\mu=1}$ for the α helix, respectively. The parameter W_{n+1n} determines the value of the intrachain transfer matrix element establishing ET from one peptide unit to the neighboring ones across the hydrogen bonds on a strand of index μ.

The local part of the vibrational Hamiltonian models an intramolecular (intrapeptide) vibrational degree of freedom, constituted by the amide-I vibration of each peptide unit. The dynamics of the intramolecular vibrations is described by a set of harmonic oscillators each situated at a site of index $(n\mu)$,

$$H_{intra}=\sum_{n\mu}\frac{1}{2M}P^2_{n\mu}+\frac{M\Omega^2}{2}\sum_n Q^2_{n\mu}, \tag{2}$$

with $P_{n\mu}$ and $Q_{n\mu}$ being the momentum and coordinate, respectively, corresponding to the displacement of the oscillator from its equilibrium position. M is the reduced mass and Ω the frequency.

The diagonal coupling between the electronic degree of freedom and the harmonic oscillators is modeled by the interaction Hamiltonian

$$H_{e\text{-}intra}=\alpha\sum_{n\mu} Q_{n\mu}|c_{n\mu}|^2. \tag{3}$$

Due to the coupling the local electronic on-site energy $\epsilon_{n\mu} = \epsilon_0 + \alpha Q_{n\mu}$ gets vibrationally modulated and α is the electron-vibration coupling parameter. Since the mass of an intramolecular oscillator is significantly larger than that of the electron we treat the system of the intramolecular oscillators classically while we use a quantum description for the transfer of the electron. In this sense the system attributed to the Hamiltonian of Eqs. (1)–(3) represents a multistrand extension of the semiclassical one-dimensional Holstein system [33,34].

The peptide groups are treated as single mass entities allowed to move in three dimensions. The bond interactions between the peptide groups held the helix in its secondary structure. Between nearest neighboring units at $(n\mu)$ and $(n\mu \pm 1)$ covalent bonds are formed. The peptide groups situated at $(n\mu)$ and $(n \pm 1\mu)$ are linked through hydrogen bonds. The three-dimensional helix backbone (also referred to as the protein matrix) of two types of helices are sketched in Fig. 1, namely, the 3-10 [Fig. 1(a)] and the α form [Fig. 1(b)], respectively. They differ in the number of residues per turn and the height of one turn, i.e., the pitch. Additionally, they can have different diameters. There exist left-handed and right-handed helices, respectively. The helix is right-handed (left-handed) if the motion from one peptide unit to the neighboring one in positive z direction goes along with a positive (negative) angle in the x-y plane.

The geometry of the protein matrix can be described in a cylindrical coordinate system whose z axis coincides with the helix axis. The rest positions of the peptide groups are determined by

$$x_{n\mu}^{(0)} = r \cos[2\pi L/l(3n+\mu)], \tag{4}$$

$$y_{n\mu}^{(0)} = r \sin[2\pi L/l(3n+\mu)], \tag{5}$$

$$z_{n\mu}^{(0)} = (3n+\mu)l, \tag{6}$$

where l is the distance between two neighboring peptide groups located at sites $(n\mu)$ and $(n\mu \pm 1)$, respectively, measured along the axis between them, r is the peptide group-axis distance (radius of the cylinder spanning the helix) and L is the step size of the helix. The winding ratio l/L is not necessarily an integer and determines the number of residues per single loop of the helix.

Since the strong covalent bonds (bond energies on the order of 50–250 kcal/mol) are rather rigid compared to the comparatively weak and flexible H bonds (bond energies 1–7 kcal/mol) [2] it is reasonable to model the (weak) covalent bond distortions in a harmonic fashion. The vibrational dynamics of the elastic hydrogen bonds is treated anharmonically [35] and we use Morse potentials. The Hamiltonian of the intermolecular interactions is given by

$$H_{inter} = \frac{1}{2m} \sum_n \sum_\mu p_{n\mu}^2 + \sum_n \sum_\mu U_{cov}(r_{n\mu}) + U_{hyd}(s_{n\mu})$$

$$= \frac{1}{2m} \sum_n \sum_\mu p_{n\mu}^2 + \frac{1}{2}\kappa \sum_n \sum_\mu r_{n\mu}^2$$

$$+ D \sum_n \sum_\mu (1 - \exp[-a s_{n\mu}])^2, \tag{7}$$

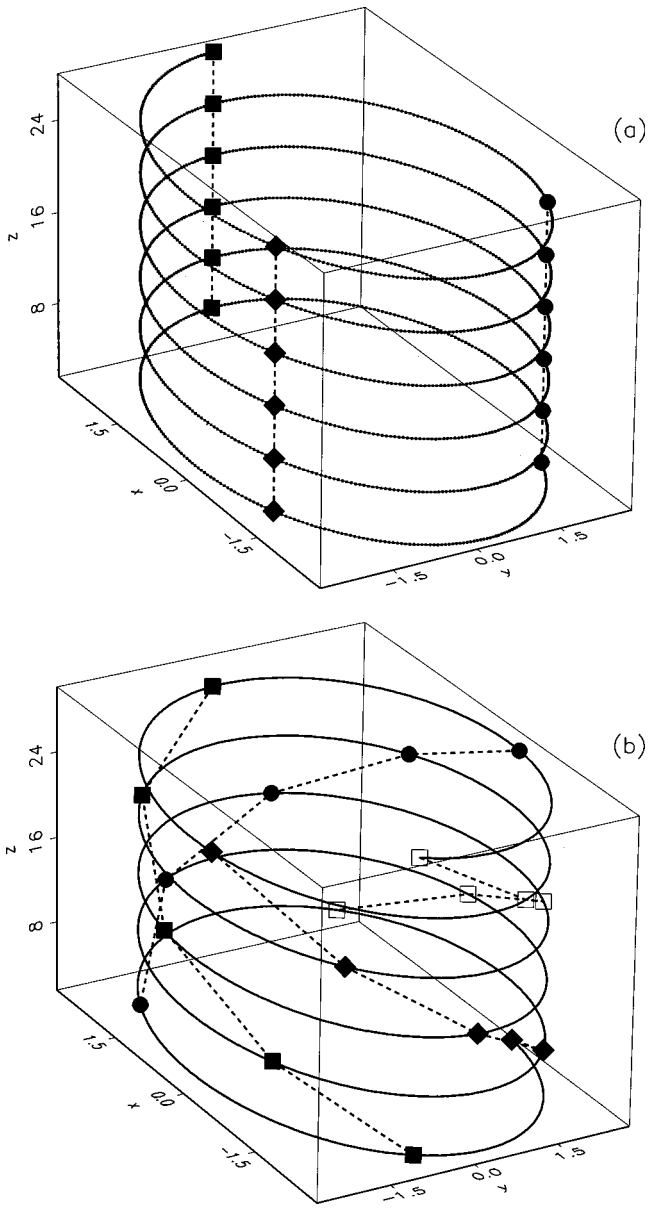

FIG. 1. Ball and stick figures of the spatial structure of the helices. Each thick symbol represents a peptide unit and equal symbols are attributed to the same μ strand. Dashed lines connecting equal symbols sketch H bonds between the peptide units of a strand. Each pair of different symbols linked by the clockwise ascending spiral curve represents peptide units of different strands connected via a covalent bond. (a) The 3-10 helix with winding ratio $l/L = 3.0$. (b) The α helix with winding ratio $l/L = 3.6$.

with the momentum vector $p_{n\mu} = (p_{n\mu}^{(x)}, p_{n\mu}^{(y)}, p_{n\mu}^{(z)})$ associated with the displacements $(x_{n\mu}, y_{n\mu}, z_{n\mu})$ of the peptide units from their equilibrium positions $(x_{n\mu}^{(0)}, y_{n\mu}^{(0)}, z_{n\mu}^{(0)})$ in x-y-z coordinates. The deviations of the covalent and hydrogen bond lengths from their equilibrium lengths $r_{n\mu}^{(0)}$ and $s_{n\mu}^{(0)}$, respectively are expressed as

$$r_{n\mu} = [(x_{n\mu} - x_{n\mu-1} + \Delta x_\mu^{(0)})^2 + (y_{n\mu} - y_{n\mu-1} + \Delta y_\mu^{(0)})^2 + (z_{n\mu} - z_{n\mu-1} + \Delta z_\mu^{(0)})^2]^{1/2} - r_{n\mu}^{(0)}, \tag{8}$$

$$s_{n\mu}=[(x_{n\mu}-x_{n-1\mu}+\Delta x_n^{(0)})^2+(y_{n\mu}-y_{n-1\mu}+\Delta y_n^{(0)})^2 + (z_{n\mu}-z_{n-1\mu}+\Delta z_n^{(0)})^2]^{1/2}-s_{n\mu}^{(0)}, \tag{9}$$

with the abbreviations

$$\Delta x_\mu^{(0)}=x_{n\mu}^{(0)}-x_{n\mu-1}^{(0)}, \quad \Delta y_\mu^{(0)}=y_{n\mu}^{(0)}-y_{n\mu-1}^{(0)},$$

$$\Delta z_\mu^{(0)}=z_{n\mu}^{(0)}-z_{n\mu-1}^{(0)}, \tag{10}$$

$$\Delta x_n^{(0)}=x_{n\mu}^{(0)}-x_{n-1\mu}^{(0)}, \quad \Delta y_n^{(0)}=y_{n\mu}^{(0)}-y_{n-1\mu}^{(0)},$$

$$\Delta z_n^{(0)}=z_{n\mu}^{(0)}-z_{n-1\mu}^{(0)}, \tag{11}$$

and

$$r_{n\mu}^{(0)}=\sqrt{(\Delta x_\mu^{(0)})^2+(\Delta y_\mu^{(0)})^2+(\Delta z_\mu^{(0)})^2}, \tag{12}$$

$$s_{n\mu}^{(0)}=\sqrt{(\Delta x_n^{(0)})^2+(\Delta y_n^{(0)})^2+(\Delta z_n^{(0)})^2}. \tag{13}$$

The parameter κ regulates the stiffness of the covalent bond chain, m is the mass of a single peptide unit, D determines the break up energy of the hydrogen bond, and a is the range parameter of the Morse potential. The point-point intermolecular interaction potentials are normalized as $U_{cov}(r_{n\mu}^{(0)})=U_{hyd}(s_{n\mu}^{(0)})=0$ and $U'_{cov}(r_{n\mu}^{(0)})=U'_{hyd}(s_{n\mu}^{(0)})=0$. Although the distortions of the covalent bonds evolves in a harmonic potential the corresponding dynamical equations are nonetheless nonlinear due to Eq. (8).

The transfer matrix elements are assumed to depend exponentially on the distance between the peptide units, that is, the length of the covalent respectively the hydrogen bonds

$$V_{\mu\mu-1}=V\exp[-\beta r_{n\mu}], \tag{14}$$

$$W_{nn-1}=W\exp[-\gamma s_{n\mu}], \tag{15}$$

with β and γ being the coupling parameters. It is through Eqs. (14) and (15) that the couplings between the electronic and bond vibrational degrees of freedom (DOF) are introduced. In this manner the transfer matrix elements are modulated by the motion of the molecular sites relative to each other.

Finally, the coupling between the intramolecular and intermolecular vibrations is incorporated in an interaction Hamiltonian

$$H_{intra\text{-}inter}=\sum_n\sum_\mu Q_{n\mu}[\chi_c(r_{n\mu+1}+r_{n\mu}) + \chi_h(s_{n+1\mu}+s_{n\mu})], \tag{16}$$

connecting each local intramolecular vibrational coordinate of a molecular site with the involved bond coordinates with χ_c and χ_h being the coupling constants. Altogether our model takes into account the exchange between electronic (more generally excitonic), intramolecular as well as intermolecular vibrational energy, respectively.

We scale the time according to $\tilde{t}=\Omega t$ and introduce the dimensionless quantities:

$$\tilde{W}=\frac{W}{V}, \quad \tilde{D}=\frac{D}{V}, \quad \tilde{Q}_{n\mu}=\sqrt{\frac{M\Omega^2}{V}}Q_{n\mu},$$

$$\tilde{P}_{n\mu}=\sqrt{\frac{M\Omega^2}{V}}P_{n\mu},$$

$$\tilde{x}_{n\mu}=\sqrt{\frac{M\Omega^2}{\lambda V}}x_{n\mu}, \quad (x_{n\mu}\leftrightarrow y_{n\mu},z_{n\mu}),$$

$$\tilde{p}_{n\mu}^{(x)}=\sqrt{\frac{\lambda}{MV}}p_{n\mu}^{(x)}, \quad (p_{n\mu}^{(x)}\leftrightarrow p_{n\mu}^{(y)},p_{n\mu}^{(z)}),$$

$$\tilde{a}=\sqrt{\frac{V\lambda}{M\Omega^2}}a, \quad (a\leftrightarrow\beta,\gamma),$$

$$\tilde{\chi}_c=\frac{\sqrt{\lambda}}{\Omega^2 M}\chi, \quad (\chi_c\leftrightarrow\chi_h,\sqrt{\lambda}\kappa), \quad \tilde{\alpha}=\frac{1}{\sqrt{VM\Omega^2}}\alpha, \tag{17}$$

with the mass ratio $\lambda=M/m$. Dropping the tildes afterwards the corresponding scaled coupled equations of motion read as

$$i\,\tau\dot{c}_{n\mu}=\alpha\,Q_{n\mu}c_{n\mu}-W\exp(-\gamma s_{n\mu})c_{n-1\mu} - W\exp(-\gamma s_{n+1\mu})c_{n+1\mu}-[\exp(-\beta r_{n\mu})c_{n\mu-1} + \exp(-\beta r_{n\mu+1})c_{n\mu+1}], \tag{18}$$

$$\dot{P}_{n\mu}=-Q_{n\mu}-\alpha|c_{n\mu}|^2-\chi_c(r_{n\mu+1}+r_{n\mu}) - \chi_h(s_{n+1\mu}+s_{n\mu}), \tag{19}$$

$$\dot{Q}_{n\mu}=P_{n\mu}, \tag{20}$$

$$
\begin{aligned}
\dot{p}^{(x)}_{n\mu} = {} & \gamma W \exp(-\gamma s_{n\mu}) \frac{(x_{n\mu} - x_{n-1\mu} + \Delta x^{(0)}_{n})}{s_{n\mu} + s^{(0)}_{n\mu}} [c^{*}_{n\mu} c_{n-1\mu} + c_{n\mu} c^{*}_{n-1\mu}] \\
& - \gamma W \exp(-\gamma s_{n+1\mu}) \frac{(x_{n+1\mu} - x_{n\mu} + \Delta x^{(0)}_{n+1})}{s_{n+1\mu} + s^{(0)}_{n+1\mu}} [c^{*}_{n+1\mu} c_{n\mu} + c_{n+1\mu} c^{*}_{n\mu}] \\
& + \beta \exp(-\gamma r_{n\mu}) \frac{(x_{n\mu} - x_{n\mu-1} + \Delta x^{(0)}_{\mu})}{r_{n\mu} + r^{(0)}_{n\mu}} [c^{*}_{n\mu} c_{n\mu-1} + c_{n\mu} c^{*}_{n\mu-1}] \\
& - \beta \exp(-\gamma r_{n\mu+1}) \frac{(x_{n\mu+1} - x_{n\mu} + \Delta x^{(0)}_{\mu+1})}{r_{n\mu+1} + r^{(0)}_{n\mu+1}} [c^{*}_{n\mu+1} c_{n\mu} + c_{n\mu+1} c^{*}_{n\mu}] \\
& - \kappa r_{n\mu} \frac{(x_{n\mu} - x_{n\mu-1} + \Delta x^{(0)}_{\mu})}{r_{n\mu} + r^{(0)}_{n\mu}} + \kappa r_{n\mu+1} \frac{(x_{n\mu+1} - x_{n\mu} + \Delta x^{(0)}_{\mu+1})}{r_{n\mu+1} + r^{(0)}_{n\mu+1}} - \chi_c Q_{n\mu} \left(\frac{(x_{n\mu} - x_{n\mu-1} + \Delta x^{(0)}_{\mu})}{r_{n\mu} + r^{(0)}_{n\mu}} \right. \\
& \left. - \frac{(x_{n\mu+1} - x_{n\mu} + \Delta x^{(0)}_{\mu+1})}{r_{n\mu+1} + r^{(0)}_{n\mu+1}} \right) - \chi_h Q_{n\mu} \left(\frac{(x_{n\mu} - x_{n-1\mu} + \Delta x^{(0)}_{n})}{s_{n\mu} + s^{(0)}_{n\mu}} - \frac{(x_{n+1\mu} - x_{n\mu} + \Delta x^{(0)}_{n+1})}{s_{n+1\mu} + s^{(0)}_{n+1\mu}} \right) \\
& - 2aD[1 - \exp(-a s_{n\mu})] \exp(-a s_{n\mu}) \frac{(x_{n\mu} - x_{n-1\mu} + \Delta x^{(0)}_{n})}{s_{n\mu} + s^{(0)}_{n\mu}} \\
& + 2aD \left[1 - \exp(-a s_{n+1\mu}) \exp(-a s_{n+1\mu}) \frac{(x_{n+1\mu} - x_{n\mu} + \Delta x^{(0)}_{n+1})}{s_{n+1\mu} + s^{(0)}_{n+1\mu}} \right., \qquad (21)
\end{aligned}
$$

$$
\dot{x}_{n\mu} = p^{(x)}_{n\mu}, \qquad (22)
$$

and the equations for the y,z components are obtained by substituting $x \leftrightarrow y,z$ in Eqs. (21) and (22), respectively. The (small) value of the adiabaticity parameter $\tau = \hbar\,\Omega/V$ expresses the time scale separation between the fast intramolecular vibrations and the slow intermolecular ET. Note that through a simple phase transformation $\tilde{c}_n(t) = c_n(t)\exp[-i\,\epsilon_0 t]$ the ϵ_0 dependence has been removed from the electronic equation of motion.

The parameter values used throughout this study lie in the range of realistic quantities for proteins [1,2,19,22]: $V \simeq 2.5$ eV, $W \leqslant 1.0$ eV, $D = (0.04\text{–}0.3)$ eV, $m \simeq 100 \times m_{proton}$, $\Omega = 3.11 \times 10^{14}\mathrm{s}^{-1}$, $a = \beta = \gamma = (1\text{–}2)$ Å^{-1}, $\kappa = (0.35\text{–}1.77)$ eV/Å^2 and $\chi_c \simeq \chi_h \simeq 40 \times 10^{-3}$ eV/Å^2. The geometry of the 3-10 helix is determined by a pitch 6 Å, distance $l = 2.0$ Å and radius $r = 3.0$ Å and the parameters of the α helix are given by pitch 5.4 Å, distance $l = 1.5$ Å and radius $r = 2.8$ Å. For the present investigation we fix the scaled parameters as $V = 1$, $D = 0.02$, $a = \beta = \gamma = 0.1$, $\kappa = 0.001$, $\chi_c = \chi_h = 0.001$, $\lambda = 0.1$ and $\tau = 0.1$. The dispersion parameter $W < 1$ and the electron-vibration coupling strength α are varied.

III. STATIONARY SOLUTIONS AND POLARONS

Since the couplings of the intermolecular vibrations to the electron motion as well as the intramolecular DOF's are supposed to be weak compared to the coupling between the electron and the intramolecular vibrations we consider as a first step the restricted problem of the ET dynamics independent of the vibrations of the protein matrix. The physical justification for the separate consideration of the restricted ET dynamics is also given by the time scale hierarchy according to which the intramolecular processes evolve much faster than any intermolecular motion involving changes of the coordinates of the heavy peptide units. In particular when the protein gets initially excited due to phototransfer an excess electron may exchange energy rapidly with the local intramolecular vibrations such that a polaron can be formed. The subsequent interaction of the polaron with the adjacent bonds is then considered in Sec. IV.

The system of the coupled electron and intramolecular vibrations is derived from the Hamiltonian of Eqs. (1)–(3) for $\beta = \gamma = \chi_c = \chi_h = 0$. Particularly the distance-independent transfer matrix elements become constant, i.e., $W_{nn-1} = W$ and $V_{\mu\mu-1} = V$. In the following we construct polaron solutions of the coupled electron vibration system whose scaled equations of motion read as

$$
i\,\tau \dot{c}_{n\mu} = \alpha\, Q_{n\mu} c_{n\mu} - (c_{n\mu-1} + c_{n\mu+1}) - W(c_{n-1\mu} + c_{n+1\mu}), \qquad (23)
$$

$$
\ddot{Q}_{n\mu} = -Q_{n\mu} - \alpha |c_{n\mu}|^2. \qquad (24)
$$

This coupled system can be viewed as a multistrand extension of the standard (one-dimensional) semiclassical Holstein model of mere nearest-neighbor-interaction that is covered in the limit case of $W = 0$. To obtain polaron states we

consider the corresponding stationary system. With the condition $\dot{Q}_{n\mu}=0$ one gets the instantaneous displacements

$$Q_{n\mu}=-\alpha|c_{n\mu}|^2. \tag{25}$$

Substituting Eq. (25) and inserting the ansatz

$$c_{n\mu}=\psi_{n\mu}\exp(-iEt) \tag{26}$$

in Eq. (23), respectively, results in a nonlinear difference system

$$E\psi_{n\mu}=-[\psi_{n\mu+1}+\psi_{n\mu-1}]-W[\psi_{n+1\mu}+\psi_{n-1\mu}] -\alpha^2|\psi_{n\mu}|^2\psi_{n\mu}, \tag{27}$$

for the time-independent amplitudes $\psi_{n\mu}$.

Let us recall that in the one-dimensional Holstein system, when the shape of the polaron solution depends only on the parameter α there exists always a (unique) polaron solution as the ground state of the system. Moreover, the transition from large to small polarons proceeds smoothly and the larger the coupling strength α the more localized and the higher in amplitude the wave functions become [33,36,37].

A. Variational approach

In order to gain analytical insight into the nature of the polaron states under the impact of longer-range couplings for W we use a simple trial function to produce variational results. We choose

$$\psi_{n\mu}=A\,\eta^{|n|+|\mu-\mu_0|}, \tag{28}$$

where the variational parameter $0<\eta<1$ gives the width of the solution. The closer η is to the value $\eta\to 1$ the more delocalized becomes the state and in the extreme case $\eta=1$ the state is fully extended. Correspondingly, for $\eta\to 0$ the state gets more localized. We present the details of the investigations for the 3-10 helix. The analysis of the α helix is performed in an analogous way and we conclude Sec. III B with a comparison between the localization properties of the two helix types.

The coefficient A follows from the normalization condition $\Sigma_{n\mu}|\psi_{n\mu}|^2=1$ and is evaluated as

$$A=\sqrt{\frac{1-\eta^2}{(1+\eta^2)(1+2\eta^2)}}. \tag{29}$$

The total variational energy Γ is computed by substituting the ansatz (28) into

$$\Gamma=-\frac{\alpha^2}{2}\sum_{n\mu}|\psi_{n\mu}|^4-\sum_{n\mu}[\psi^*_{n\mu}\psi_{n\mu-1}+\psi_{n\mu}\psi^*_{n\mu-1}] -W\sum_{n\mu}[\psi^*_{n\mu}\psi_{n-1\mu}+\psi_{n\mu}\psi^*_{n-1\mu}], \tag{30}$$

resulting in

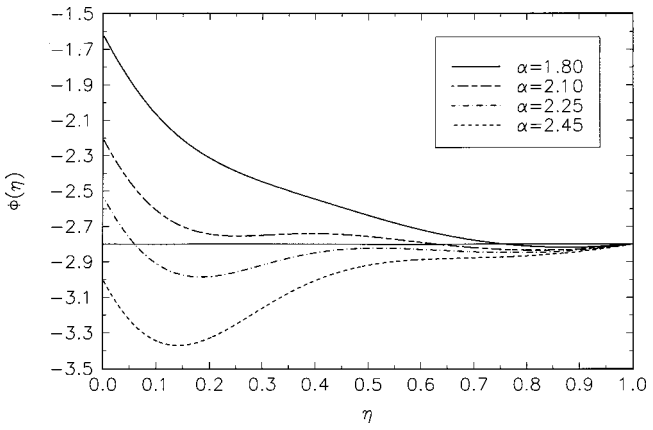

FIG. 2. The variational energy Γ defined in Eq. (31) as a function of the variational parameter η for $W=0.4$ and selected values of α as indicated in the plot. Upon increasing α a transition from a single well via a double well back to a single well potential takes place.

$$\Gamma(\eta)=-4\frac{\eta}{1+\eta^2}(1+W\,\eta^2[2-\eta^2]) -\frac{\alpha^2}{2}\frac{(1-\eta^2)(1+\eta^4)}{(1+\eta^2)^3}. \tag{31}$$

In Fig. 2 we show the function $\Gamma(\eta)$ for selected values of α and fixed $W=0.4$. The straight line marks the lowest energy of the extended states. We recall that for $W=0$ the function $\Gamma(\eta)$ exhibits only a single minimum corresponding to a stable polaron as the ground state of the lattice system. On the contrary upon increasing the electron-vibration interaction α for a given $W>0$ there occur transitions from a single minimum at large η via two minima back to a single minimum of $\Gamma(\eta)$ at small η. In the illustrated case of $W=0.4$ we observe that for values of $\alpha\leqslant 2.05$ there exists a single minimum of Γ lying below the energy of the extended states. Since the location of this minimum is at a large value of η it is attributed to a large polaron ground state. For intermediate values $2.05<\alpha\leqslant 2.20$ a second minimum above the extended state energy appears for small η implying the existence of a metastable small polaron state. The large polaron still represents the ground state. Further increasing of α leads to simultaneous lowering of the left minimum and raising of the right one. Eventually for $\alpha\geqslant 2.40$ there remains only one single minimum of Γ and the larger α is the closer is the location of this gradually deepened minimum to the value $\eta=0$. Consequently, with enlarged α not only the degree of localization is enhanced but also the amplitude of the small polaron becomes higher. On the other hand, this localization effect is the more suppressed the larger the value of W is taken.

B. Construction of polaron solutions

We construct the polaron solutions numerically following the method outlined in Refs. [36,37]. To this end one utilizes that polarons (localized electronic states in companion with

vibrational displacements localized in the same lattice region) are obtained as the attractors of the map

$$\{\psi\} \rightarrow \{\bar{\psi}\} = H\{\psi\}/\|H\{\psi\}\|, \tag{32}$$

with

$$\{\psi\} = \begin{pmatrix} \psi_{1\mu=1}, \psi_{2\mu=1}, \ldots, \psi_{N\mu=1} \\ \psi_{1\mu=2}, \psi_{2\mu=2}, \ldots, \psi_{N\mu=2} \\ \psi_{1\mu=3}, \psi_{2\mu=3}, \ldots, \psi_{N\mu=3} \end{pmatrix}, \tag{33}$$

where the operator H is determined by the right hand side of Eq. (27) and the norm of the state $H\{\psi\}$ is defined as $\|H\{\psi\}\| = \sqrt{\Sigma_{n\mu}(H\{\psi\})^2}$.

As one initial condition for the map iterations we take a completely localized state, i.e., $\{\psi_{n\mu}^{(0)}\} = \delta_{n,n_0\mu,\mu_0}$, and act on it with the operator H. After each application of H the resulting vector is normalized and the iteration procedure is terminated when convergence is attained yielding the polaron state. Inspired by the results gained from the variational approach we use completely delocalized initial conditions, characterized by $\{\psi_{n\mu}^{(0)}\} = 1/\sqrt{3N}$, as well. In dependence of the initial conditions the map (32) may possess two distinct attractors and the lattice supports either a small or a large polaron solution separated from each other by an energetic barrier. The small polaron attractor is approached starting from the localized initial conditions and corresponds to the minimum of $\Gamma(\eta \rightarrow 0)$ while the other attractor attributed to the large polaron minimum of $\Gamma(\eta \rightarrow 1)$ is approachable with delocalized initial conditions.

For an illustration of the influence of the longer-range dispersion W on the formation of polarons and their stability properties we plot in Fig. 3 the total energy of the polaron defined as

$$E_{polaron} = -\frac{\alpha^2}{2}\sum_{n\mu}|\psi_{n\mu}|^4 - \sum_{n\mu}[\psi_{n\mu}^*\psi_{n\mu-1} + \psi_{n\mu}\psi_{n\mu-1}^*]$$

$$-W\sum_{n\mu}[\psi_{n\mu}^*\psi_{n-1\mu} + \psi_{n\mu}\psi_{n-1\mu}^*], \tag{34}$$

as a function of α for different values of W. For $W=0$, when the transition from large to small polarons is smooth, the graph of E shows a monotone decay with growing α. However, for $W>0$ we find that in certain α intervals the initial conditions corresponding to a completely localized state and to a completely extended state yield different energies. For the sake of proper notations we call in the following the polarons constructed from completely extended (localized) initial conditions *e polarons* (*l polarons*) and use furthermore the term α *polaron* (3-10 *polaron*) for the polaron state of the α helix (3-10 helix).

The results for the variational energy Γ have predicted that in some ranges of α a small and a large polaron exist for equal parameters. The graphs in Fig. 3 confirm the bistability feature present whenever the long-range interaction parameter W is greater than zero. Bistability arising through long-range interaction was also found in one-dimensional chain models. In Ref. [38] the effects of long-range harmonic interactions in a one-dimensional chain with short-range anharmonicity was considered. It was shown that the existence of two velocity-dependent length scales leads to two types of solitons with different widths (small and large polarons) for two velocity regions separated by a gap. Furthermore, for a nonlinear discrete Schrödinger equation with long-range dispersive interaction the existence of bistability in the solution behavior was observed in [39]. The two existing stable stationary states represent a continuumlike soliton and an intrinsically localized mode. Bistability was further observed in the solutions of a one-dimensional molecular chain with a periodic on-site potential [40]. It was shown that the polaron state exists only for appropriate system parameters while a delocalized exciton state can always exist. The latter constitutes in some parameter regions a stable ground state and is in other cases metastable leaving the polaron as the ground state. In our study of the multistrand Holstein system we find that there exists always at least one polaron and in dependence on the coupling strength α either the small or large polaron forms the ground state of the system.

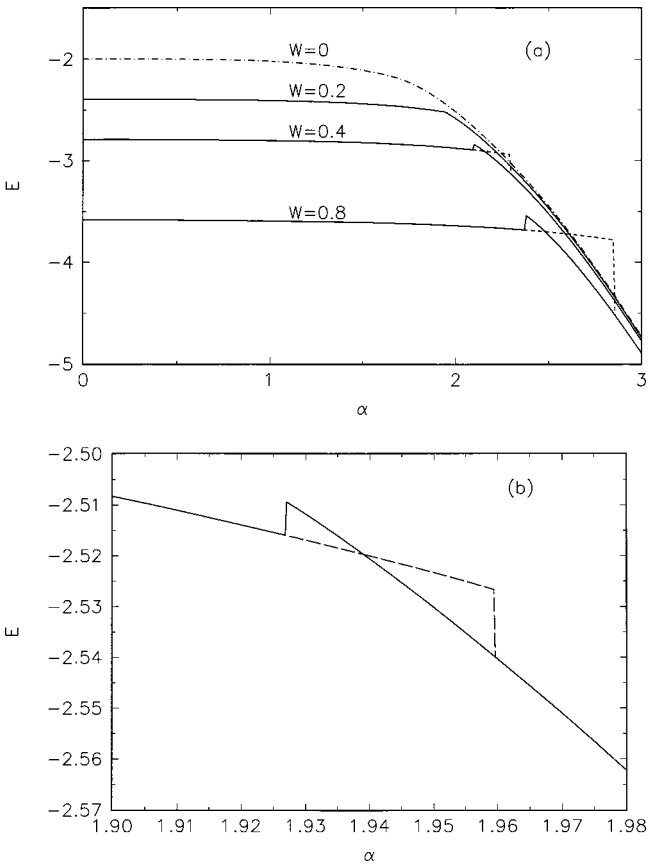

FIG. 3. The total polaron energy as a function of the electron-vibration coupling α. (a) For different values of W as indicated in the figures. The full (dashed) lines belong to *l* polarons (*e* polarons) of the 3-10 helix. (b) Detailed plot of the transition region for $W=0.2$ showing the vertical ascent of the l-polaron energy followed by its crossing of the *e*-polaron level and the return of the *e*-polaron energy to the *l* branch when α is increased.

Figure 3(b) reveals the details of the enlarged transition region of the polaron energy for $W=0.2$. At a critical value

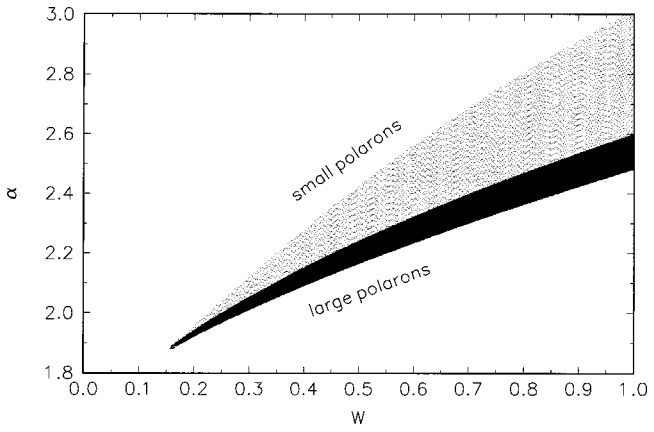

FIG. 4. Illustration of the bistability of the polaron solutions in the W-α-parameter plane for the 3-10 helix. The dark (gray shaded) area designates parameters for which the l polaron energy is greater (smaller) than the e polaron energy. Accordingly, in the dark (gray shaded) region the ground state is formed by the e polaron (l polaron).

$\alpha_1 = 1.927$ the energy of the l polarons (full line) abruptly jumps to a value above the e polaron (dashed line) and two separate energy branches appear for $\alpha > \alpha_1$. We stress that for the illustrated case of $W = 0.2$ the energy of the small polarons remains below the lowest extended state energy so that the small polarons cannot become metastable. (Metastability occurs only for overcritical $W \geqslant 0.4$.) Enlarging α causes that the small as well as the large polaron energies are steadily lowered although the decline of the small polaron energy is much stronger. In fact, above a critical value $\alpha_2 = 1.939 > \alpha_1$ the small polaron energy falls off one of the large polaron reversing the energetic relations, i.e., now the small polaron forms the ground state. Furthermore, at a larger critical value $\alpha_3 = 1.960 > \alpha_2$ the large polaron energy makes a sudden rejoining drop to the level of the small polaron to continue with the same course for $\alpha > \alpha_3$. In general, enhanced dispersion W hinders the formation of small polarons. Particularly, the greater the W the more the onset of the bistability transition is shifted towards larger α values. Moreover, in the domain of bistability the energetic barrier between the lower-energy small (medium) polarons and the large ones is raised with growing W.

We remark that we found good agreement between the results obtained from the analytical variational approach and the numerical map method with respect to the polaron energy and the pattern of the wave function. (In the large polaron range sometimes a hyperbolic secant shape for the trial functions yields even more accurate results than the exponential ansatz.)

The parameter dependence of the bistability property of the multistrand polaron model is properly illustrated in the W-α plane presented in Fig. 4 where the dark area represents the region of such parameter constellations for which the small l-polaron energy lies above the ones of the large (medium) e polarons while the latter constitute the ground state. Conversely, the gray shaded area marks the parameter range for which the large e-polaron energy exceeds the small l polaron energy level leaving the small l-polarons in the ground state. Note that with increased dispersion W both regions expand. Particularly, the large (medium) polaron ground states sustain stronger electron-vibration couplings and their existence and stability range is extended towards higher α values. This parameter dependence is of importance for the polaron dynamics (considered below in Sec. III D) because large (medium) polarons are supposed to be mobile. Below the dark area the polarons are of large and medium extension whereas above the gray shaded area we encounter exclusively small polarons.

Typical wave functions assigned to the different stability regions are depicted in Fig. 5. A large polaron is seen in Fig. 5(a) belonging to the ground state for $\alpha = 1.0$. Figures 5(b) and 5(c) illustrate for $\alpha = 1.93$ the bistability issue connected with the possibility of the excitation of the higher-energy small polaron state (l polaron) and the medium polaron ground state (e polaron) for the same parameters. At last in Fig. 5(d) the small polaron ground state is shown for $\alpha = 2.0$ exhibiting not only pronounced localization with respect to the n direction but also strong exponential concentration of the pulse on a single μ strand.

In Fig. 6 we demonstrate the impact of longer-range dispersion on the degree of localization by plotting the energetic partition number defined as

$$\overline{E}_{polaron} = \frac{\left(\sum_{n\mu} E_{polaron} \right)^2}{\sum_{n\mu} E_{polaron}^2}, \tag{35}$$

where the polaronic energy is defined by Eq. (34). The polaronic energy is completely confined at a single site if $\overline{E}_{polaron} = 1$ and is uniformly extended over the lattice if $\overline{E}_{polaron}$ is of the order $3N$. Thus $\overline{E}_{polaron}$ measures how many sites are excited to contribute to the lattice energy. Apparently the larger the electron-vibration coupling α the more dominates the on-site potential term $\alpha^2/2\Sigma_{n\mu}|\psi_{n\mu}|^4$ the total polaron energy diminishing the role played by the nonlocal dispersive part. In reverse, when the overall dispersion is enlarged with growing W the influence of the nonlocal dispersive term is amplified hindering small polaron formation. Hence, the situation of equipartition is favored. Below a critical value α' the e polarons and l polarons coincide so that they possess identical partition numbers. However, at the overcritical α' the equipartition number of l polarons jumps discontinuously uplinked with an abrupt large-small polaron transition giving birth to a small l-polaron branch of the partition number (full lines). (To guide the eyes a vertical line going from the transition point on the lower branch to the upper one is drawn.) The lower branch of the large e polaron (lower dashed lines) is prolongated till the critical value α'' at which the sudden onset of the large-small e-polaron transition appears. For $\alpha > \alpha''$ the small e polarons and l polarons are again identical possessing equal partition numbers. To relate the current results with preceding ones we quote that the values of the transition points α' and α''

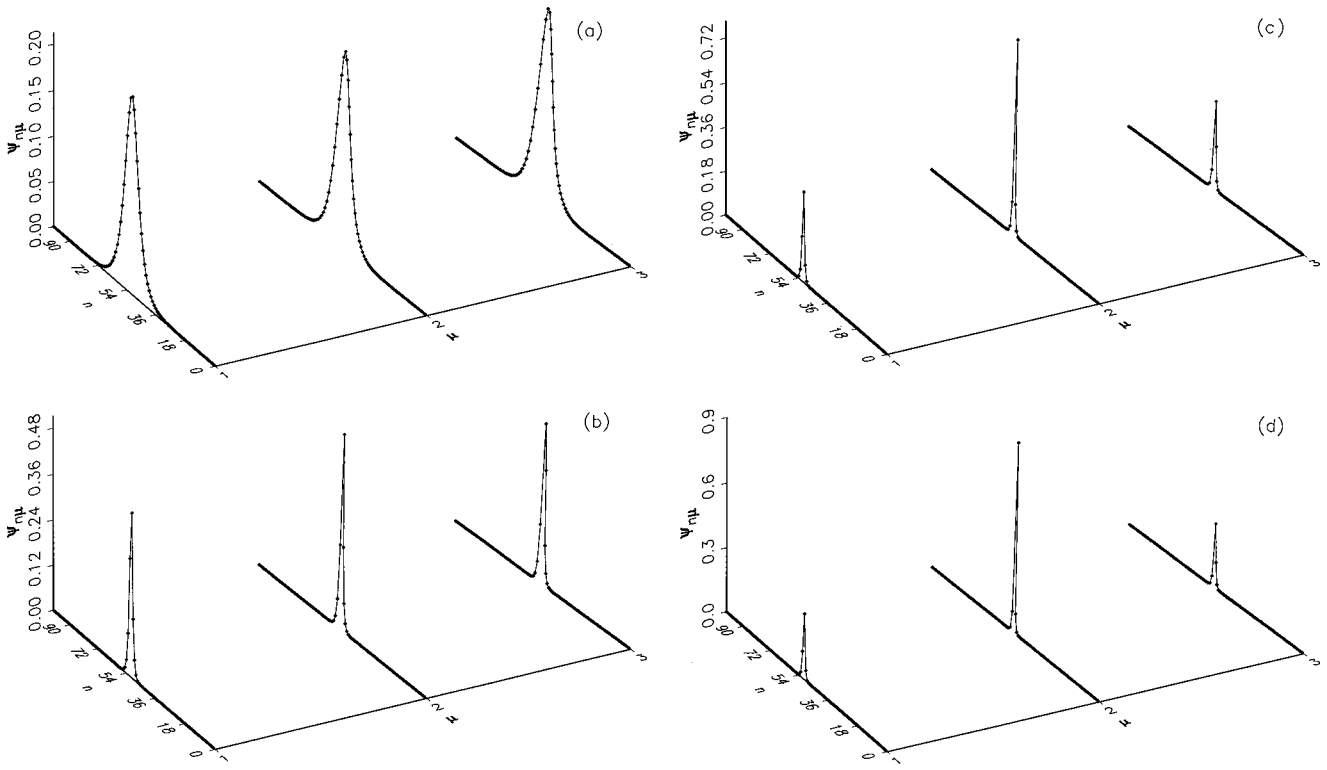

FIG. 5. Polaron wave functions for $W=0.2$ and different values of α for the 3-10 helix. (a) Large polaron for $\alpha=1.0$. (b) Bistability: The e polaron for $\alpha=1.93$. (c) Bistability: The l polaron. Parameter α as in (b). (d) Small polaron for $\alpha=2$.

are given for $W=0.2$ by $\alpha'=\alpha_1=1.939$ and $\alpha''=\alpha_3=1.960$ in agreement with the polaron energy transitions displayed in Fig. 3(b).

We conclude this section with a comparison of the localization properties of the 3-10 polarons and α polarons. In Fig. 7 we plot the wave function of a standard, 3-10 and α polaron, respectively for equal coupling parameter α. We use one-dimensional representations for which the helix backbones are viewed as if as extended as possible. The spatial index $m=1,\ldots,3N$ $(m=1,\ldots,4N)$ is uniquely related to the 3-10 helix (α helix) index pair $(n\mu)$ through $m=3n-(3-\mu)$ $[m=4n-(4-\mu)]$, $\mu=1,\ldots,3$ $(\mu=1,\ldots,4)$ and $n=1,\ldots,N$. We recognize that of all three polarons the standard polaron $(W=0)$ is the most narrow one and generally for a chosen value of $W>0$ the 3-10 polaron is of smaller extension than the α polaron. Further, the larger W is taken the smaller gets the height of the central polaron amplitude. Moreover, we state that the large-small polaron transition is performed at a larger coupling strength α for the 3-10 polaron than for the α polaron.

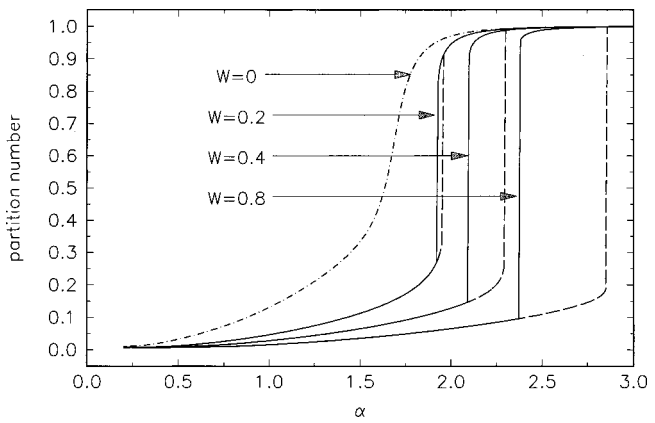

FIG. 6. The energetic partition number defined in Eq. (35) as a function of α. The curve parameter W is indicated in the plot. For $W>0$ the full (dashed) line corresponds to the partition numbers of the l polarons (e polarons) of the 3-10 helix.

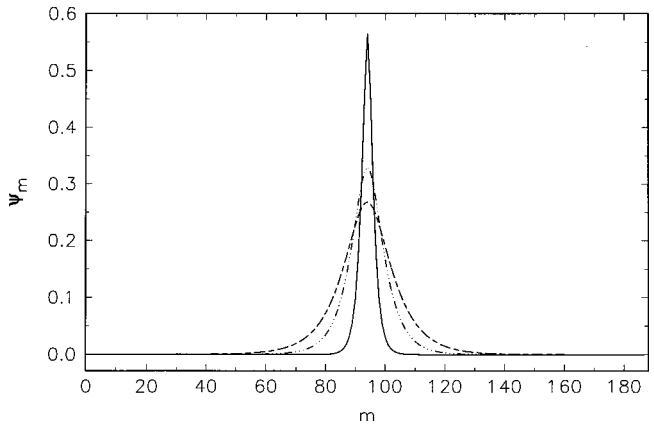

FIG. 7. Wave function for the standard (full line), the 3-10 (dotted-dashed line) and α polaron (dashed line), respectively, with parameters $\alpha=1.5$ and $W=0.2$ except for $W=0$ for the standard polaron.

C. Polaron normal modes

In this section we investigate the linear stability of the polarons focusing interest on the existence of localized internal modes. The latter play a fundamental role for the formation, stability, and mobility of breathers [41–47]. We impose small perturbations

$$Q_{n\mu}(t) = Q_{n\mu}^{(0)}(t) + \delta Q_{n\mu}(t), \tag{36}$$

$$c_{n\mu}(t) = \{\psi_{n\mu} + \delta c_{n\mu}(t)\} \exp\left[-i\frac{E_e}{\tau}t\right], \tag{37}$$

where $\delta Q_{n\mu}$ and $\delta c_{n\mu}$ are small quantities and E_e is the electronic energy of the stationary state. Substituting Eqs. (36) and (37) into the system (23),(24) and linearizing around ($Q_{n\mu} = Q_{n\mu}^{(0)}$ and $c_{n\mu} = \psi_{n\mu}$) gives the linear system of tangent equations

$$i\,\tau \delta \dot{c}_{n\mu} = \alpha(Q_{n\mu}^{(0)} \delta c_{n\mu} + \delta Q_{n\mu}\psi_{n\mu}) - (\delta c_{n\mu+1} + \delta c_{n\mu-1}) - W(\delta c_{n+1\mu} + \delta c_{n-1\mu}), \tag{38}$$

$$\delta \ddot{Q}_{n\mu} = -\delta Q_{n\mu} - \alpha(\psi_{n\mu}\delta c_{n\mu}^{*} + \psi_{n\mu}^{*}\delta c_{n\mu}). \tag{39}$$

Introducing the perturbation vector $\Delta = (\delta c_{n\mu}, \delta c_{n\mu}^{*}, \delta Q_{n\mu}, \delta \dot{Q}_{n\mu})$ we express the system (38),(39) in matrix notation

$$\dot{\Delta} = M\,\Delta, \tag{40}$$

where the periodic entries of the Jacobian matrix $M = M(\psi_{n\mu}, \psi_{n\mu}^{*}, Q_{n\mu}^{(0)}(t), \dot{Q}_{n\mu}^{(0)}(t))$ follow from the evolution of system (23),(24). For an analysis of the system (40) we proceed in a standard way using Floquet theory. To this end we integrate the equations of motion over one period $T = 2\pi\tau/E_e$ to get the Floquet map

$$\Delta(T) = F\,\Delta(0), \tag{41}$$

giving the evolution of an initial deviation of the periodic solution after one period T with the Floquet matrix F. Linear stability requests that all the eigenvalues $R_n \exp(i\Theta_n)$ of F lie on the unit circle. Additionally the Floquet analysis provides us with the frequencies of the normal modes via the relation $\omega_\Theta = \omega_e \Theta/(2\pi)$ with Θ expressed in *rad*.

Intensive numerical investigations in a wide parameter range have proved that all the polarons gained from the map (32) are linearly stable. We underline that also in the regime of bistability the *l* polarons as well as the *e* polarons are stable. The α and 3-10 polarons exhibit similar spectral features. Therefore we restrict the representation to the 3-10 polaron. A typical spectrum of the Floquet eigenvalues is shown in Fig. 8 for $\alpha = 1.9$ and $W = 0.2$. For later quotation the inset displays the velocity component of the pinning mode in a one-dimensional representation.

In Fig. 9 we present the frequencies of the lowest breathing and pinning modes as a function of the electron-vibration coupling α for different values of the transfer matrix element W. In Figs. 9(a) and 9(b) the cases $W = 0$ and $W = 0.2$ for a lattice with periodic boundary conditions when the only attractor of the map (32) originates from localized initial conditions, are shown. The dashed (full) line represents the pinning (breathing) mode. The pinning mode is the lowest frequency mode for undercritical values of α. For the standard case ($W = 0$) the large-small polaron transition is reflected in a crossing of the two branches so that the breathing mode becomes the lower one [36,37]. For the extended polaron system with $W > 0$ the beginning of the existence range of the localized internal modes is shifted to higher α values. Below a critical α_c the behavior of the standard case is resembled. At the critical α_c the low-frequency antisymmetric pinning mode converts to symmetric parity and the lowest mode goes steadily over into a breathing mode. At the same time, the original breathing mode branch ceases to exist. Concerning the pinning mode, at α_c there appears a frequency gap between its original branch and the higher-frequency continuation above the new breathing mode. This discontinuous exchange between the pinning and moving mode positions has to be distinguished from the steady mode crossing taking place in the standard case.

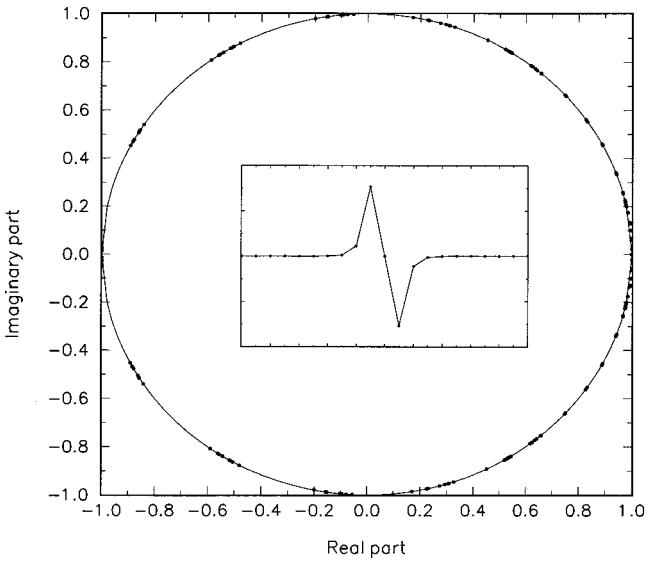

FIG. 8. Distribution of the Floquet eigenvalues on the unit circle for the 3-10 helix. Parameters: $\alpha = 1.9$ and $W = 0.2$. The inset displays the antisymmetric pattern of the velocity component of the pinning mode.

In Figs. 9(c)–9(e) results for the polaron lattice with open boundary conditions, for which the completely localized and extended initial conditions may lead to polaron solutions, are illustrated. In the standard case [Fig. 9(c)] the large-small polaron transition is connected with the usual mode crossing for which the breathing mode becomes the lower one for large α. However, with $W > 0$ there appears richer structure in the spectra. One observes that from the lower frequency pinning mode at a value α_1 a breathing mode branch bifurcates off. (In the remainder of this section we refer to the breathing and pinning modes for $\alpha < \alpha_1$ as the original modes.) The newly developed breathing mode continues above the original pinning mode and crosses at α_2 the original higher-frequency breathing mode. The latter drops down

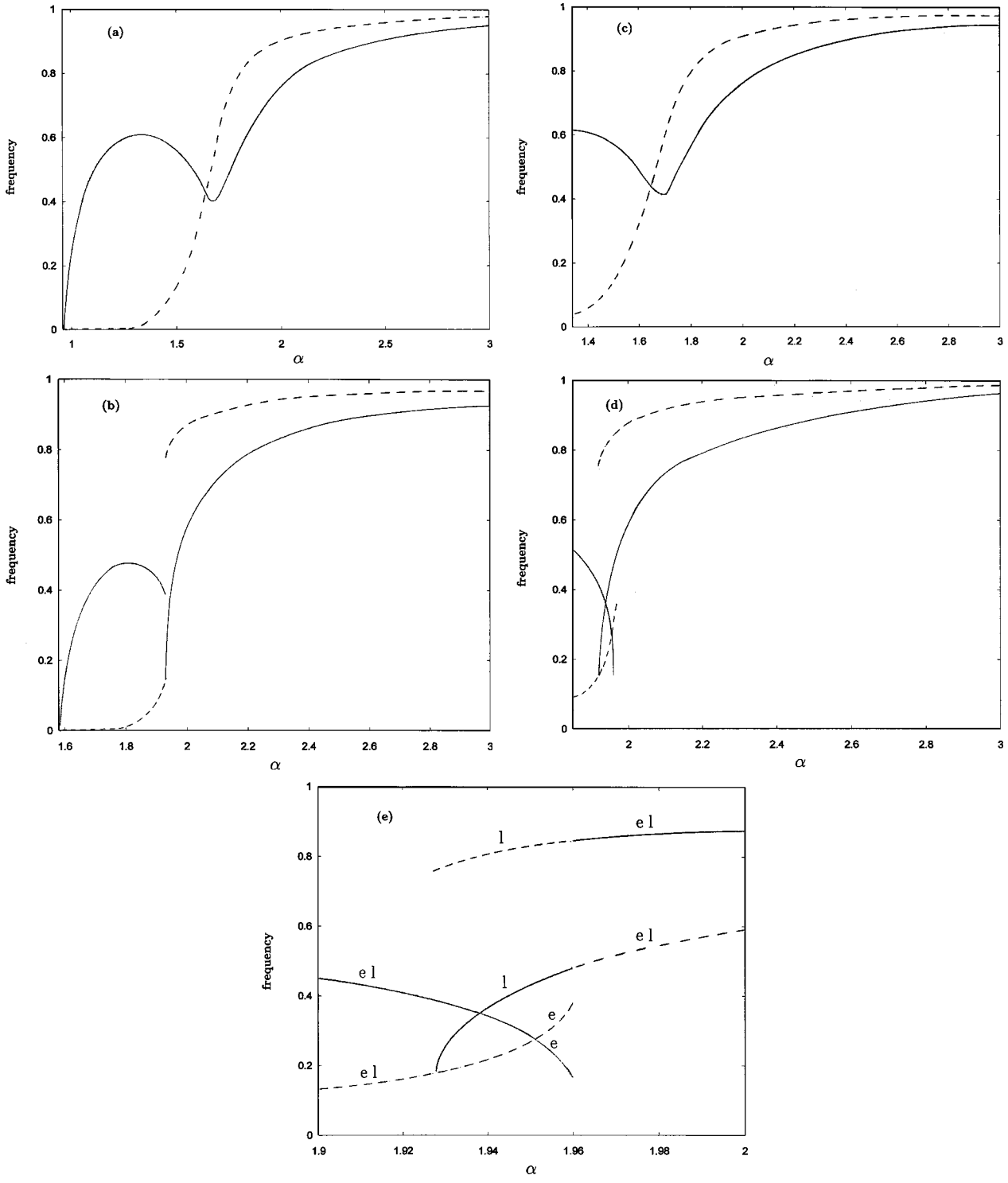

FIG. 9. Frequencies of the breathing and pinning modes as a function of α and given values of W. A breathing (pinning) mode is represented by the solid (dashed) line, respectively. (a) The standard case $W=0$ for periodic boundary conditions. (b) As in (a) except for the longer-range dispersion $W=0.2$. (c) As in (a) but for open boundary conditions. (d) As in (c) except for $W=0.2$. (e) Details of the transition region of (d). Assignments of the branches of different line types to the *l* polaron (l) and *e* polaron (e) as indicated in the plot.

in frequency as α grows and terminates simultaneously with the lower pinning mode at a value α_3.

For a more detailed explanation of the transitions associated with the different behavior of the *e* polarons and *l* polarons we show details of the transition region in Fig. 9(d). We use the prefixes *e* and *l* not only to label the two polaron types but also to distinguish the localized internal modes attributed to them. Furthermore we emphasize that the three transition points $\alpha_{1,2,3}$ determining the bistability, energetic and localization features of the polarons as illustrated in

Figs. 3 and 6, respectively, are directly related to the spectral properties of the corresponding localized internal modes.

The original pinning mode branch (the lowest dashed line section) belongs for $\alpha_1<1.927$ to an internal localized mode of the coinciding large size *e* polarons and *l* polarons. At $\alpha_1=1.927$ a breathing mode bifurcates off the original *l* branch and continues as the full line above the continued *e*-pinning mode while the *l*-pinning mode jumps abruptly up in frequency (upper dashed line). Hence, the lowest mode of the *l* polaron is now supported by a breathing mode (lowest full line section). This mode exchange is related to the sudden transition from a large to a small *l* polaron. The latter possesses higher energy content than its *e*-polaron counterpart and thus the region of bistability for which the *e* polaron forms the ground state is entered at $\alpha_1=1.927$ (compare Figs. 3(b) and 4, respectively). However, the continued *e*-pinning mode branch (the lowest dashed line) is still lower in frequency than its *e* breathing counterpart and therefore the *e* polaron retains its large size. This *e*-pinning mode crosses the e-breathing mode branch (full line) at $\alpha'=1.951$ from below and terminates at $\alpha_3=1.960$ when it performs a jump up in frequency to merge with the *l*-pinning mode branch (upper dashed line). Physically, in the interval $\alpha'<\alpha<\alpha_3$ the lower mode of the *e* polaron is now of breathing type rendering the size of the *e* polaron from large to medium or even small. Similar bifurcation behavior is found concerning the original breathing mode, that is, below $\alpha_1=1.927$ the *l* branch and the *e* branch coincide (full line). At α_1 the *l* branch terminates and is for $\alpha>\alpha_1$ continued as the breathing *l* mode that has bifurcated off the original *l*-pinning mode branch as described above. Thus, equivalent to the discontinuous continuation of the *l*-pinning mode with its jump up in frequency the *l*-breathing mode performs a sudden jump down in frequency. The steady prolongation of the original breathing *e* mode goes further down in frequency as α grows and crosses the off-bifurcated breathing *l* mode at $\alpha_2=1.939$. Note that beyond this point the energy of the *l* polaron drops below the *e*-polaron energy level. Hence, the former constitutes the ground state [see Fig. 3(b)]. After the original branch of the *l*-breathing mode has intersected the branch of the original *l*-pinning mode it stops at α_3. For $\alpha>\alpha_3$ the *e* polaron and *l* polaron coincide and share common branches of breathing and pinning modes, respectively. Opposite to the behavior in the interval $\alpha<\alpha_1$ the breathing mode is now the lower frequency mode so that the polarons are of small extension.

D. Moving polarons

In this section we study the mobility of polarons facilitating a numerical method originally developed for breather solutions [41]. (Actually, the electronic amplitude pattern $|c_{n\mu}|^2$ can be regarded as a static electron breather solution Ref. [42].) According to [41] we initiate the motion of polarons through suitable perturbations of the velocity variables $\{\dot{Q}_{n\mu}(t)\}$ targeted in the direction of the pinning mode. To be precise, we use for the numerical integration of the system (23),(24) the following initial conditions:

$$\{\psi_{n\mu},0,Q^{(0)}_{n\mu},0\}+k\{0,0,0,\xi\}, \tag{42}$$

with the normalized velocity part ξ of the pinning mode and *k* is the perturbation strength. Due to the lattice discreteness the polarons are pinned and have to overcome a certain Peierls-Nabarro-energy barrier in order to become mobile along the discrete lattice [43]. Mobility is achieved for overcritical perturbation strengths *k* as long as the (stationary) polaron extension is not too small [36,44,37].

We exploited the lowest frequency pinning mode although others of higher frequency can be applied too. The time-evolution of a mobile polaron for the standard case $W=0$ and $\alpha=1.5$ kicked initially with the velocity component of its pinning mode is displayed in Fig. 10(a). Taking into account a longer-range dispersion $W>0$ and keeping α fixed leads to a broadening of the (stationary) polaron profile. That greater polaron extension does not necessarily imply higher pulse velocity can be seen in Fig. 10(b). In comparison with the preceding standard case [Fig. 10(a)] the present polaron moves with smaller but uniform velocity along the lattice and its localized shape remains invariant. We have also varied the value of α such that the polarons for the cases $W=0$ and $W=0.1$ have equal stationary profile, respectively. For example the constellation $W=0$ and $\alpha=1.15$ exhibits a stationary profile equal to the corresponding one for $W=0.1$ and $\alpha=1.5$. Interestingly, the comparison of the Figs. 10(c) and 9(c) reveals that the incorporation of longer-range dispersion improves the polaron mobility. Unlike the immobile polaron for $W=0$ the corresponding one for $W=0.1$ moves along the lattice. We remark that qualitatively equal results are obtained for the mobility of the α polarons.

IV. THE COUPLED POLARON BOND-VIBRATIONS SYSTEM

In this section we study the ET problem when the polaron system is coupled to the vibrations of the protein matrix oscillators. Due to their mutual couplings energy exchange between electronic, intramolecular, and intermolecular degrees of freedom may take place. According to the preceding findings (see Sec. III C) the polaron as the stationary and linearly stable solution of the system (23),(24) is the ground state of the polaron system. On the other hand, an initially highly nonequilibrium situation occurs when a localized electron (polaron) is produced by initial excitation of the protein due to phototransfer. This polaron can distribute parts of its energy into the bonds till energy equilibration is attained. With the perspective to ET we pay special attention to the existence and stability of moving polarons when the motion is induced by local vibrations of the protein matrix. To this end we initialized the system (18)–(22) with a bare *small* polaron state derived in Sec. III. All oscillators (peptide units) of the protein matrix are initially held in their rest positions. However, the impact of the electronic terms on the bond oscillators in Eq. (21) lead to immediate deformations of the bonds initiating the energy exchange dynamics.

At least two interesting questions arise; namely, will the coupled system relax to a steady regime, and second, what is the destiny of the polaron when it gets coupled to the vibra-

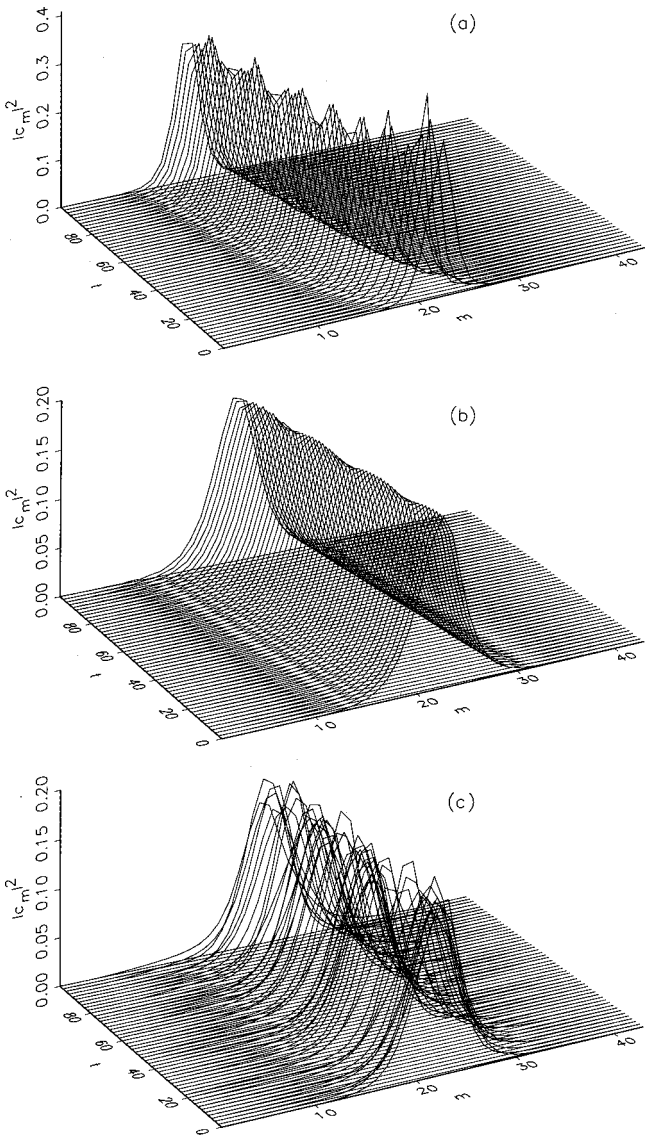

FIG. 10. Time evolution of the 3-10 polarons when the velocity component gets initially kicked in the direction of the corresponding pinning mode. The spatial index $m=1,\ldots,3N$ of the one-dimensional representation of the amplitude pattern is related to the 3-10 helix index through $m=3n-(3-\mu)$ and $n=1,\ldots,N$. (a) Moving polaron in the standard case $W=0$, $\alpha=1.5$, and $k=0.2$. (b) Moving polaron under the impact of longer-range dispersion. Parameters as in (a) except for $W=0.1$. (c) Immobile standard polaron. Parameters $\alpha=1.15$, $W=0$, and $k=0.2$. We remark that the stationary polaron shape is equal to those in (b).

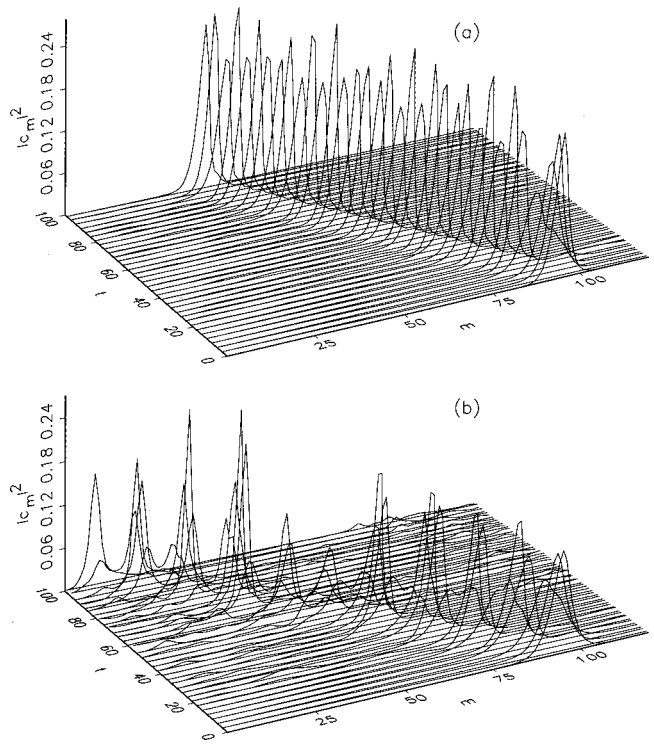

FIG. 11. The coupled polaron bond-vibrations dynamics: Time-evolution of the electron breather in a one-dimensional representation. Parameters as given in the text and $N=63$ ($N=47$) for the 3-10 helix (α helix). Note that for a better illustration only a section of the lattice is displayed. (a) The 3-10 polaron. The spatial indices of the depicted one-dimensional representation and the actual position on the strands are related via $m=3n-(3-\mu)$ with $m=1,\ldots,3N$, $n=1,\ldots,N$, and $\mu=1,\ldots,3$. (b) The α polaron with index relation $m=4n-(4-\mu)$ with $m=1,\ldots,4N$, $n=1,\ldots,N$, and $\mu=1,\ldots,4$.

tions of the protein matrix? Moreover, will the coupled dynamics still support a standing polaron or does the protein matrix dynamics even act as the ''driving'' force to activate polaron motion? Finally, can we expect a geometrical effect and does the steric arrangement of the protein matrix have consequences for the ET?

We integrated the system (18)–(22) numerically using a fourth-order Runge-Kutta method and monitored the accuracy of the numerical computations by checking the conservation of the total energy and the norm $\Sigma_{n\mu}|c_{n\mu}|^2=1$, respectively.

In order to compare the dynamical properties of the two helix types we take equal dispersion parameter $W=0.2$ in both cases and choose the coupling parameter α such that the α polaron and 3–10 polaron exhibit initially comparable patterns. Interestingly, we observe that after an initial transient phase the polaron starts to move along the lattice in a coherent fashion as illustrated in Figs. 11(a) [11(b)] for the *electron breather* of the 3-10 helix (α helix). Regarding the mobility the α polaron exhibits similar behavior to the 3-10 polaron. Both polaron types retain in essence their localized shape throughout the journey in the peptide lattice, which is further proved by the time evolution of the second momentum of the electronic amplitude distribution measuring the spatial extension of the electron profile shown in Fig. 12. However, the α polaron exhibits larger temporary spreadings of its width than the 3-10 polaron clearly reflected in the amplitudes of the second momenta. The evolution of the first momentum of the amplitude distribution portrayed in Fig. 13 affirms that the polarons move almost coherently in time but the α polaron moves faster than the 3-10 polaron but motion of the α polaron sets in earlier. Furthermore, the first momentum remains zero in the initial phase corresponding to a resting polaron and the motion sets in more or less abruptly

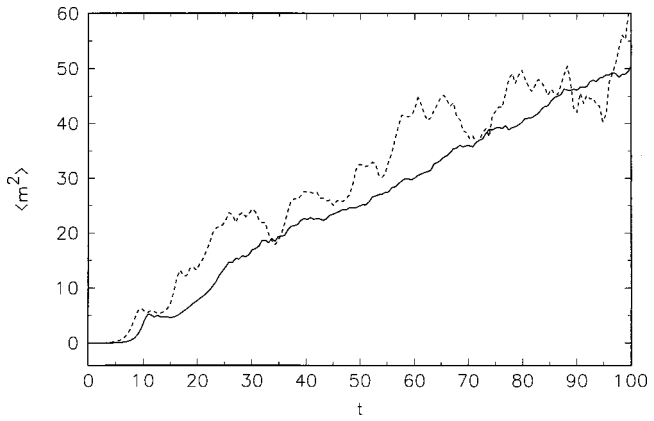

FIG. 12. Time-evolution of the second momentum of the electronic amplitude distribution $|c_{n\mu}|^2$ for the 3-10 helix (solid line) and the α helix (dashed line).

at an instant of time pointing to a kicklike initiation of the motion.

Let us remind that the kinetic energy of the bare polaron is zero. This situation changes when the coupling to the protein matrix is taken into account. The coupled system is no longer in an equilibrium state and the relaxation dynamics induces energy transmission. During the initial phase when the polaron still rests (zero and/or not enough kinetic energy to overcome the mobility threshold) a steady directed flow of small amounts of polaron potential energy into the bond DOF's takes place mainly at the site of the polaron center. This temporary potential energy loss of the polaron, at most amounting to 5% of the total polaron energy, broadens effectively the polaron profile. At the same time when the bonds receive energy at the expense of the polaron energy they get distorted from their initial rest positions. More precisely, when amounts of the initial polaron energy are conveyed into the bond degrees of freedom a standing *bond-breather* at the central position of the bare polaron is created. The nonlinear terms contained in the equations of motion of the bond oscillators are responsible that on receipt the majority of the energy does not disperse away from the absorbing site. In reverse, due to the coupling between the intermolecular and intramolecular oscillators [cf. the term $-\chi_c(r_{n\mu+1}+r_{n\mu})-\chi_h(s_{n+1\mu}+s_{n\mu})$ in Eq. (19)] the deformations of the bonds react on the polaron system so that the polaron's momentum is no longer zero. Additionally, due to possibly developed deviations from the stationary polaron profile the term $-Q_{n\mu}-\alpha|c_{n\mu}|^2$ may no longer vanish as it used to be for the bare polaron and thus could contribute to further alterations of the polaron momentum.

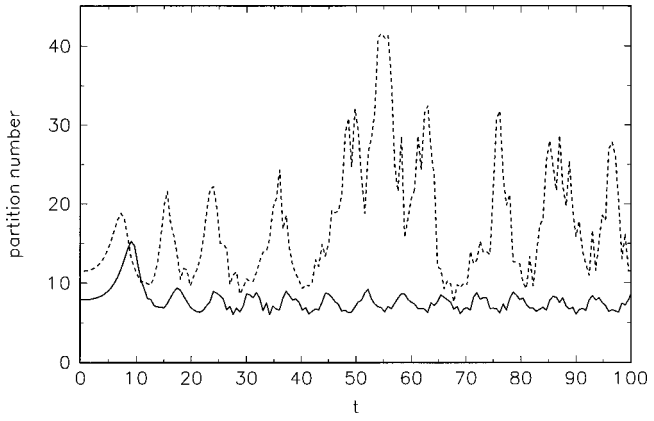

FIG. 13. Time-evolution of the first momentum of the electronic amplitude distribution $|c_{n\mu}|^2$ for the 3-10 helix (solid line) and the α helix (dashed line).

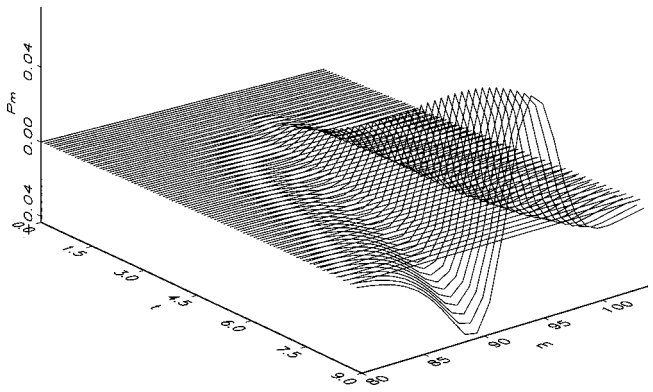

FIG. 14. The spatiotemporal pattern of the momentum $P_{n\mu}$ for the 3-10 helix in the initial phase during which the antisymmetric shape develops.

Remarkably, as Fig. 14 reveals a consistently growing velocity component of the polaron develops resembling the antisymmetric shape of a pinning mode. Eventually, at a certain instant of time the size of the internally created antisymmetric velocity component has become large enough to initiate motion of the meanwhile further enlarged polaron. We observe that the ET takes place solely via the strongly coupled short covalent bonded units (covalent path) and the interchain transfer via the weak and extended H bonds is suppressed. We tested also polaronic states on a single strand consisting of hydrogen bonded units as initial conditions. However, no coherent polaron motion on a hydrogen path could be observed.

After the polaron motion has been activated the coupled dynamics continues in a (quasi)stationary regime characterized by the uniformly traveling polaron and the standing bond breathers. In general, we find that the pattern of the α polaron exhibits larger spatiotemporal oscillations than the 3-10 polaron pointing to a heavier energy exchange between the polaron and the protein matrix vibrations in the α helix. In Fig. 15 we illustrate the evolution of the excitation patterns of the covalent as well as hydrogen bonds. In fact, the protein matrix of the 3-10 helix absorbs less amount of polaronic energy than its corresponding α helix counterpart. After the polaron has passed a region the encompassed hydrogen bonds get stretched and pinned bond breathers are developed whose positive maximal amplitude is the smaller the further apart the bond breather is from the starting site. The covalent bonds stay permanently stretched once the polaron has encountered them. The percentage of the total energy contained finally in the bond breathers is less than two. For the α helix all covalent bonds and hydrogen-bonds become deformed in the course of the relatively fast dispersion of bond excitations into the whole lattice. These bond defor-

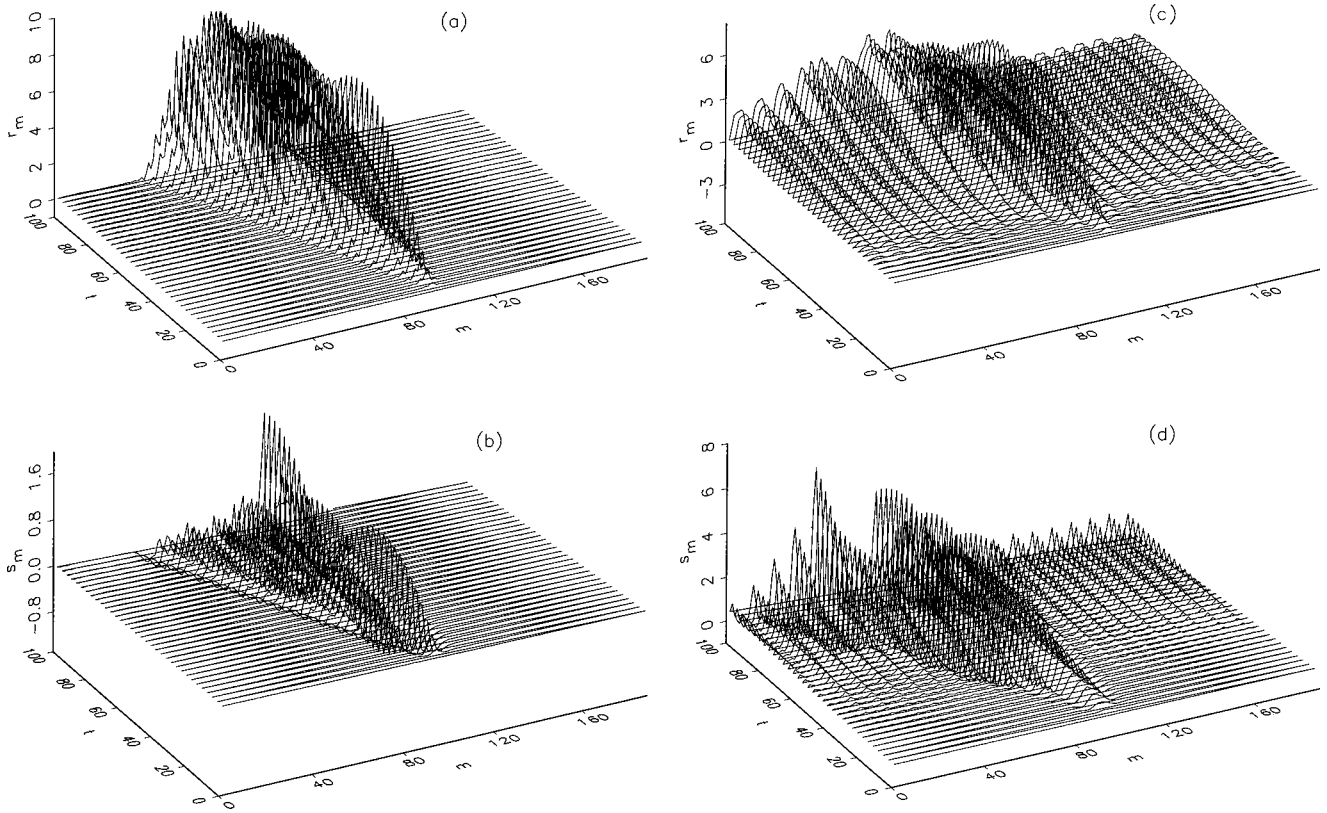

FIG. 15. The spatiotemporal evolution of the covalent respectively hydrogen bonds. (a) The covalent bonds of the 3-10 helix. (b) The hydrogen bonds of the 3-10 helix. (c) The covalent bonds of the α helix. (d) The hydrogen bonds of the α helix.

mations form breather lattices [48,49] built up from a variety of neighboring pinned narrow breathers. The bond breathers contained in the region not traversed by the polaron store altogether less than 0.1% of the initial polaron energy while the remaining part of the breather lattice along which the polaron travels contains approximately 4% of the total energy.

Furthermore we recognize that the amplitudes of the covalent bond breathers are of the same order for both types of helices. However, the H bonds of the α helix [Fig. 15(d)] are more susceptible to energy absorption than their rather rigid 3-10-helix counterparts [Fig. 15(b)]. This gives the reason for the comparatively heavy energy exchange between the α polaron and its protein matrix reflected also in the temporal evolution of the polaron energy

$$E_{pol} = -\sum_{n\mu} \{\alpha^2/2|c_{n\mu}|^4 + [c^*_{n\mu}c_{n\mu-1} + c_{n\mu}c^*_{n\mu-1}] + W[c^*_{n\mu}c_{n-1\mu} + c_{n\mu}c^*_{n-1\mu}]\}$$

is shown in Fig. 16. After the initial reduction the 3-10-polaron energy fluctuates around a constant mean value while the α-polaron energy keeps gradually and slowly decreasing. Obviously, the α-polaron has to ''sacrifice'' more of its energy to the bonds than the 3-10 polaron in order to maintain energy storage and to support coherent ET. Evidently, the 3-10 polaron transports its energy more efficiently than its α counterparts do.

In summary, out of a nonequilibrium situation the energy sharing between the polaron and the protein matrix proceeds such that the coupled dynamics relaxes onto solutions of coexisting electron and vibron breathers (see [52] and references therein). Hence the breathers play the role of ''attractors'' [50,51] providing a stable equilibrium state. Finally, we remark that there is no difference between left- and right-

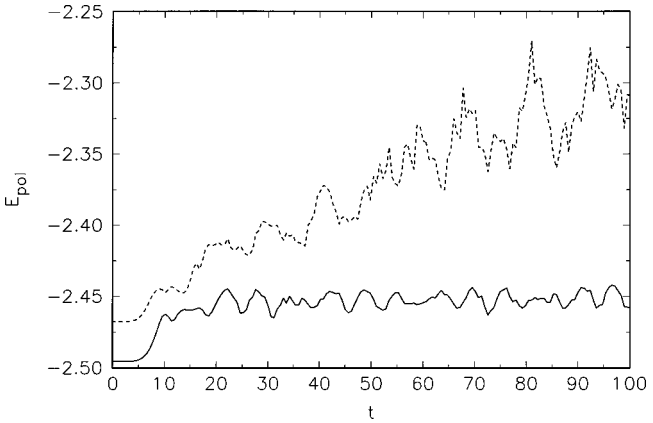

FIG. 16. Temporal evolution of the polaron energy for the 3-10 polaron (solid line) and the α polaron (dashed line).

handed helices with regard to the coupled polaron protein matrix dynamics.

V. SUMMARY

In this paper we have considered the ET in the context of helical protein models. The steric arrangement of the protein secondary structure is modeled by a three-dimensional oscillator network. The hydrogen and covalent bond interactions between the peptide groups are modeled via pair potentials. Each peptide group has an internal vibrational degree of freedom representing the amide-I mode. The motion of the electron over the peptide groups is described by a tight-binding system. The various dynamical degrees of freedom are mutually coupled making the exchange of electronic, intramolecular, and intermolecular vibrational energy, respectively, possible.

With view to the formation of self-trapped states we have studied the polaron problem described by the electronic subsystem strongly coupled to the intrapeptide amide-I vibrations. We have discussed the modification of the polaron states when longer-range dispersions arising via the hydrogen-bonded units are taken into account. First, we have used a variational method to infer on the wave pattern, energy as well as multiplicity of polaron states, respectively. Interestingly, the variational approach has resulted in bistability in the polaron solutions, that is, for the same set of parameters there are two different polarons excitable, namely, a small and a large one. This bistability phenomenon is not present in the standard polaron problem of $W=0$. In fact, this analytically predicted bistability has been verified in the ''exact'' polaron solutions derived numerically as the attractors of a map. Generally, we have found that the greater the value of the longer-range dispersion W the larger becomes the size of the stationary polaron. Comparing the localization features of the two helix types we have observed that the 3-10 helix provides stronger degree of localization than its α counterpart does.

We have further studied dynamical aspects of polarons such as their linear stability and mobility. To investigate the stability of the polarons we have linearized the system of equations of motion yielding the tangent equations. The Floquet map has been derived and it has been shown that all Floquet eigenvalues are located on the unit circle guaranteeing linear stability. In addition the Floquet analysis has provided us with the frequencies of the normal modes of the polarons. We have discussed the impact of longer-range dispersion $(W>0)$ on the existence and stability of localized internal polaron modes. In the large polaron regime the lowest internal localized mode is presented by a pinning mode whereas the breathing mode oscillates with higher frequency. As the most striking feature we observed that at an overcritical value α_c the pinning mode branch jumps suddenly up in frequency leaving the breathing mode as the lowest localized internal mode. This discontinuous mode exchange is related to the sudden transition from a large to a small polaron and has to be distinguished from the gradual large-small-polaron transition related with the steady mode crossing in the standard polaron problem.

In the regime when the polarons are of large (medium) extension we have initiated polaron motion by kicking the velocity component in the direction of the corresponding pinning mode. Remarkably, the incorporation of longer-range dispersion may improve the polaron mobility and we have found constellations for which the standard polaron remains immobile whereas for the corresponding polaron of equal size for $W>0$ motion can be activated.

In the second part of the paper we have considered the steric dynamical problem of the polaron system interplaying with the vibrational degrees of freedom of the protein matrix. We have numerically integrated the corresponding coupled equations of motion initializing the polaron subsystem with a stationary small (and initially immobile) polaron state. Starting in a nonequilibrium initial state we have focused attention on the relaxation dynamics in the energy exchange and the initiation of polaron motion. Generally, the polaron maintains a localized shape and keeps the majority of its energy content. Nevertheless, some amount of the potential polaron energy is locally transferred into the bond vibrations. During an initial transient phase the energy transfer is spatially confined to the central position of the polaron because the nonlinearity contained in the bond equations prevents a dispersion of the conveyed energy. Accordingly, we observe the creation of a pinned breather on the hydrogen bond as well as on the covalent-bond lattice, respectively. In a feedback manner the newly generated bond breathers react locally on the momentum component of the polaron. This leads to an increase of localized kinetic polaron energy and in particular a small localized velocity component develops resembling the shape of an antisymmetric pinning mode. (We underline that initially the kinetic energy content of the polaron is zero.) Simultaneously, the width of the polaron is enlarged due to further transmission of potential polaron energy into the bonds. This combined effect of growing polaron extension and increased gain of polaron kinetic energy terminates at a certain instant of time and culminates in the activation of polaron motion. Eventually, the coupled polaron bond vibrations dynamics has reached a (quasi)stationary regime and the polaron propagates coherently along the lattice while the bonds exhibit coexisting pinned and moving breathers. We have found that the 3-10 polaron moves slower than its α counterpart but possesses the better ability to retain its energy content and localized shape.

We stress the crucial role played by the protein matrix oscillators as the medium ''mediating'' between the polaron's potential and kinetic energy contents so that precisely such amount of the polaron's potential energy is deposited into kinetic ones which is necessary to activate polaron motion. Therefore the incorporation of the spatial secondary protein structure into the polaron problem proves to be vital for the electron propagation mechanism illustrating the strong relation between structure and functional processes in biomolecules.

ACKNOWLEDGMENT

The author acknowledges support by the Deutsche Forschungsgemeinschaft via the Heisenberg program (He 3049/1-1).

[1] J.A. McCammon and S.C. Harvey, *Dynamics of Proteins and Nucleic Acids* (University Press, Cambridge, UK, 1987).
[2] C. Branden and J. Tooze, *Introduction to Protein Structure* (Garland, New York, 1991).
[3] B. Alberts, D. Bray, J. Lewis, M. Raff, K. Roberts, and J.D. Watson, *Molecular Biology of the Cell* (Garland, New York, 1983).
[4] D.N. Beratan, J.N. Onuchic, and J.J. Hopfield, J. Chem. Phys. **86**, 4488 (1987); D.N. Beratan, J.N. Betts, and J.N. Onuchic, Science **252**, 1285 (1991).
[5] J.N. Onuchic, D.N. Beratan, J.R. Winkler, and H.B. Gray, Annu. Rev. Biophys. Biomol. Struct. **21**, 349 (1992).
[6] J.J. Hopfield, Proc. Natl. Acad. Sci. U.S.A. **71**, 3649 (1974).
[7] J.J. Hopfield, J.N. Onuchic, and D.N. Beratan, Science **241**, 817 (1988).
[8] D.N. Beratan, J.N. Onuchic, and J.J. Hopfield, J. Chem. Phys. **86**, 4488 (1987).
[9] J.N. Onuchic and D.N. Beratan, J. Chem. Phys. **92**, 722 (1990).
[10] J.N. Onuchic, P.C.P. Andrade, and D.N. Beratan, J. Chem. Phys. **95**, 1131 (1991).
[11] S.S. Skourtis and D.N. Beratan, JBIC, J. Biol. Inorg. Chem. **2**, 378 (1997).
[12] H.B. Gray and J.R. Winkler, Annu. Rev. Biochem. **65**, 537 (1996).
[13] C. Turrò, C.K. Chang, G.E. Leroi, R.I. Cukier, and D.G. Nocera, J. Am. Chem. Soc. **114**, 4013 (1992).
[14] K. Schulten and M. Tesh, Chem. Phys. **158**, 421 (1991).
[15] M.H. Vos, M.R. Jones, C.N. Hunter, J. Breton, J.-C. Lambry, and J.-L. Martin, Biochemistry **33**, 6759 (1994).
[16] L.D. Landau, Phys. Z. Sowjetunion **3**, 664 (1933).
[17] S.I. Pekar, J. Phys. (Moscow) **10**, 341 (1946); **10**, 347 (1946).
[18] A.S. Davydov, J. Theor. Biol. **38**, 559 (1973); A.S. Davydov and N.I. Kislukha, Sov. Phys. JETP **44**, 571 (1976); A.S. Davydov, Sov. Phys. Rev. B **25**, 898 (1982).
[19] A.S. Davydov, *Solitons in Molecular Systems* (Reidel, Dordrecht, 1985); J. Theor. Biol. **38**, 559 (1973).
[20] *Davydov's Soliton Revisited*, edited by P.L. Christiansen and A.C. Scott (Plenum Press, New York, 1991).
[21] *Nonlinear Excitations in Biomolecules*, Proceedings of the International School, Les Houches 1994, edited by M. Peyrard (Springer-Verlag, Berlin, 1995).
[22] A.C. Scott, Phys. Rep. **217**, 1 (1992).
[23] O.H. Olsen, M.R. Samuelsen, S.B. Petersen, and L. Nørskov, Phys. Rev. A **38**, 5856 (1988).
[24] A.V. Zolotaryuk, P.L. Christiansen, and A.V. Savin, Phys. Rev. E **54**, 3881 (1996).
[25] P.L. Christiansen, A.V. Zolotaryuk, and A.V. Savin, Phys. Rev. E **56**, 877 (1997).
[26] A.V. Zolotaryuk, K.H. Spatschek, and A.V. Savin, Phys. Rev. B **54**, 266 (1996), and references therein.
[27] S. Caspi and E. Ben-Jacob, Europhys. Lett. **47**, 522 (1999).
[28] S.W. Englander, N.R. Kallenbach, A.J. Heeger, J.A. Krumhansl, and S. Litwin, Proc. Natl. Acad. Sci. U.S.A. **77**, 7222 (1980).
[29] M. Peyrard and A.R. Bishop, Phys. Rev. Lett. **62**, 2755 (1989).
[30] G. Gaeta, C. Reiss, M. Peyrard, and T. Dauxois, Riv. Nuovo Cimento **17**, 1 (1994).
[31] Q. Xie, G. Archontis, and S.S. Skourtis, Chem. Phys. Lett. **312**, 237 (1999).
[32] E.S. Medvedev and A.A. Stuchebrukhov, J. Chem. Phys. **107**, 3821 (1997).
[33] T.D. Holstein, Ann. Phys. (N.Y.) **8**, 325, 343 (1959).
[34] A. S. Alexandrov and N. Mott, *Polarons and Bipolarons* (World Scientific, Singapore, 1995).
[35] S. Yomosa, Phys. Rev. A **32**, 1752 (1985).
[36] G. Kalosakas, S. Aubry, and G.P. Tsironis, Phys. Rev. B **58**, 3094 (1998).
[37] N.K. Voulgarakis and G.P. Tsironis, Phys. Rev. B **63**, 14 302 (2001).
[38] Yu.B. Gaididei, N. Flytzanis, A. Neuper, and F.G. Mertens, Phys. Rev. Lett. **75**, 2240 (1995).
[39] Yu.B. Gaididei, S.F. Mingaleev, P.L. Christiansen, and K.Ø. Rasmussen, Phys. Rev. E **55**, 6141 (1997).
[40] Y. Zolotaryuk and J.C. Eilbeck, Phys. Rev. B **63**, 054302-1 (2001).
[41] D. Chen, S. Aubry, and G.P. Tsironis, Phys. Rev. Lett. **77**, 4776 (1996).
[42] D. Hennig and G.P. Tsironis, Phys. Rep. **307**, 333 (1999), and references therein.
[43] S. Flach and C.R. Willis, Phys. Rep. **295**, 181 (1998).
[44] Y. Zolotaryuk, P.L. Christiansen, and J.J. Rasmussen, Phys. Rev. B **58**, 14 305 (1998).
[45] M. Johansson and S. Aubry, Nonlinearity **7**, (1997).
[46] T. Cretegny and S. Aubry, Phys. Rev. B **55**, 11 929 (1997).
[47] C. Baesens, S. Kim, and R.S. MacKay, Physica D **113**, 242 (1998).
[48] J.L. Marin and S. Aubry, Nonlinearity **9**, 1501 (1996).
[49] S. Aubry, Physica D **103**, 1 (1997).
[50] M. Peyrard, Physica D **119**, 184 (1998).
[51] G.P. Tsironis and S. Aubry, Phys. Rev. Lett. **77**, 5225 (1996); A. Bikaki, N.K. Voulgarakis, S. Aubry, and G.P. Tsironis, Phys. Rev. E **59**, 1234 (1999).
[52] D. Hennig, Phys. Rev. E **62**, 2846 (2000).